Available online at www.sciencedirect.com
SCIENCE DIRECT®
International Journal of Heat and Mass Transfer 49 (2006) 2412–2419
International Journal of HEAT and MASS TRANSFER
www.elsevier.com/locate/ijhmt

Constructal theory of droplet impact geometry

A. Bejan [a], D. Gobin [b,*]

[a] Duke University, Department of Mechanical Engineering and Materials Science, Durham, NC 27708-0300, USA
[b] FAST – UMR 7608 (CNRS – Univ. Paris VI and XI), Bât. 502, 91405 Orsay, France

Received 5 July 2005; received in revised form 5 January 2006
Available online 29 March 2006

Abstract

In this paper we rely on the constructal law of maximization of flow access in order to construct a theory of geometry generation (selection, evolution) during molten droplet impact. We show that immediately after impact the liquid spreads inviscidly as a ring with a radial velocity that scales with the initial impact velocity. If the initial droplet is small and slow enough, the 'splat' comes to rest (dies) viscously, as a disc. If the droplet is large and fast enough, the ring splashes and is continued outward by needles that grow radially until they are arrested by viscous effects. We optimized the number of needles such that the total splash time is minimum. The theoretical dimensionless group that governs the selection of geometry (G) is the ratio of two lengths, the final radius of the disc that dies viscously, divided by the radius of the still inviscid ring that just wrinkles. Splats form when $G \leqslant \mathrm{O}(1)$ and splashes are favored when $G \geqslant \mathrm{O}(1)$. Experimental measurements reported in the literature confirm several of the features of the constructal development of splat vs. splash flow architecture.

Keywords: Constructal theory; Geometry generation; Selection; Evolution; Molten droplet; Splashing; Splat; Spray coating; Fingering; Forensic medicine; Blood splatter

1. Introduction

One of the puzzles regarding molten droplet behavior when impacting a dry smooth solid surface is why sometimes droplets spread as discs when they hit a solid wall, and why sometimes they 'splash' by shooting liquid as jets, fingers and smaller droplets in selected directions. The question of flow morphology—to understand the generation of shape and structure and to predict it—is enormously important. There are many applications where droplet impact behavior spells success or failure, especially in new technologies based on using small scale droplets for spray coating with molten metal, spray painting and printing, forensic medicine (blood splatter), injection systems and thin-film coatings. This question is important fundamentally as well, because without a pure theory for why both types of droplet impact behavior are observed there is no hope for the development of predictive numerical tools, and for robust correlations to guide future design and sizing of manufacturing processes.

The experimental and theoretical progress on droplet impact behavior was reviewed extensively in a recent paper by Haferl et al. [1], among others, and because of this it is not reviewed again here. The main thread of this new body of knowledge is that the two types of post-impact behavior (disc vs. splash) have been observed and documented extensively. Attempts have been made to report these observations on flow regime maps involving the dimensionless groups revealed by dimensionless analyses invoking the Buckingham π-theorem, for example, the Reynolds number (Re), Weber number (We) and Ohnesorge number (Oh)—all such numbers being based on the properties of the spherical liquid droplet before impact (see Nomenclature).

Observations show that the flow-map boundary between droplets that splash and droplets that do not splash can be described by correlations of the type $Oh^m Re^p = \text{constant}$,

* Corresponding author.
E-mail address: gobin@fast.u-psud.fr (D. Gobin).

0017-9310/$ - see front matter © 2006 Elsevier Ltd. All rights reserved.
doi:10.1016/j.ijheatmasstransfer.2006.02.001

Nomenclature

A	finger cross-sectional area, m^2
D	droplet diameter, m
g	gravitational acceleration, m/s^2
G	geometry selection number, Eqs. (39) and (40)
K	constant, $We^{1/2}Re^{1/4}$ at the transition between disc growth and splashing
L	needle length, m
m	exponent
n	number of needles, or fingers
Oh	Ohnesorge number, $We^{1/2}/Re$
p	exponent
P	pressure, Pa
r	radial dimension, m
Re	Reynolds number, VD/ν
S	ring cross-sectional area, m^2
t	time, s
u	radial velocity scale, m/s
U_a	radial velocity of the liquid in the ring, m/s
V	droplet initial velocity, m/s
We	Weber number, $\rho DV^2/\sigma$

Greek symbols

δ	viscous penetration thickness, m
ν	kinematic viscosity, m^2/s
ρ	liquid density, kg/m^3
σ	surface tension, N/m
τ	viscous shear stress, Pa

Subscripts

max	maximum
min	minimum
opt	optimum
1	viscous end of disk-shaped development
2	start of needle formation
3	viscous end of needle growth

where the half-domain of splashing behavior is occupied by $Oh^m Re^p >$ constant [2]. More recently, Mundo et al. [3] conducted an extensive experimental program that led to a correlation of the same type, $We^{1/2}Re^{0.25} = K$ (which is the same as $Oh\,Re^{1.25} = K$), where the constant is $K = 57.7$ for a set of experiments using water, ethanol or water-sucrose-ethanol droplets impacting a smooth stainless steel substrate. More experimental data are provided by two recent theses [4,5].

Correlations that are tight, robust and confirmed by new experiments call for a theory to explain their origin, and to predict them. Mundo et al. [3] proposed such a theory, which was based on a global accounting for the conservation of liquid energy and mass during droplet impact. Their analysis generated an expression for the boundary between splashing and no splashing, which next to Oh and Re contained two additional parameters: the contact angle and the dimensionless ratio D_{max}/D, where D is the original droplet diameter and D_{max} is the maximal diameter of a liquid spreading as a disc. Mundo et al.'s formula passes through the $Oh(Re)$ data that mark the splashing/no splashing boundary, but deviates from the data when $Re < 200$ and $Re > 2000$. Furthermore, the Mundo et al. formula does not have the power-law structure of the empirical correlation $We^{1/2}Re^{0.25} = K$, in which one should note that there are two empirical constants that were determined by optimizing the curve fitting of the data: K and the exponent 0.25.

In this paper we report a purely theoretical argument that anticipates not only the observed transition between splashing and no splashing, but traces the entire scenario of droplet impact behavior to the action of the constructal law [6,7]: the flow geometry that is selected evolves in time such that it maximizes the spreading of the liquid, and accelerates the arrival of equilibrium. The predictive progress made by invoking the constructal law is reviewed in [6,7], and is not reviewed again here. In this paper, we show that everything—the time and length scales of the liquid flow before and after splashing—results from the invocation of this principle, including the power-law boundary We (Re) and its two constants K and 0.25 (the theoretical value of the latter turns out to be 1/4, analytically). Most remarkable is the fact that the analysis reported in this paper was formulated not to "derive" Mundo et al.'s correlation (the discovery of the correlation was one of the surprises of this work), rather the objective was to see whether the principle of maximization of flow access anticipates the splashing phenomenon as successfully as it did other natural flow architectures such as turbulent structure, Bénard convection and dendritic solidification [6,7], and, more recently, the architecture of the human lung [8], the hydraulic jump phenomenon [9] and the speed and frequencies (stride, flapping) of all flying, running and swimming animals [10].

From the outset, we admit that the complexity of the splashing droplet phenomenon forces us to formulate the discussion in terms of scale analysis [11]. Furthermore, complexity makes it necessary to define unambiguously the various scales of the phenomenon, which change from time to time. We have done this carefully in the following analysis, and we draw the reader's attention to the definition of the subsequent time scales (t_1, t_2, t_3) and on the scenario that emerges.

2. Scale analysis of ring-shaped flow

Consider a spherical liquid droplet of diameter D, viscosity μ and density ρ, which impacts a solid wall. The

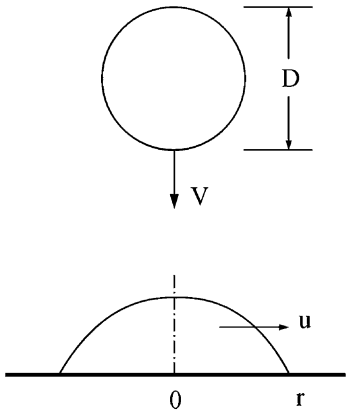

Fig. 1. Droplet parameters before and during spreading on the wall.

droplet velocity V is perpendicular to the wall at $r = 0$, as shown in Fig. 1. The liquid droplet becomes a splat that spreads on the wall. We are interested in the scales (length, time) and the morphology of the splat. This means that the following scenario refers to times longer than the initial time interval of splat deformation ($t \sim D/V$), during which the droplet touches the wall and is deformed.

Let $t = 0$ mark the moment when the splat is born on the wall. This movement is indicated by the deformed droplet shown in the lower part of Fig. 1. The stagnation of the liquid causes an instantaneous excess pressure on the order of

$$P \sim \frac{1}{2}\rho V^2 \tag{1}$$

This pressure drives the splat liquid to the distance r, which is the instantaneous radius of the splat. We assume that immediately after $t = 0$ the splat is symmetric about the $r = 0$ axis, and its flow is inviscid. The momentum equation in the r direction is

$$\rho\left(\frac{\partial u}{\partial t} + u\frac{\partial u}{\partial r}\right) = -\frac{\partial P}{\partial r} \tag{2}$$

where u is the liquid velocity component in the r direction. From kinematics, the radial velocity scale is

$$u \sim \frac{r}{t} \tag{3}$$

According to the method of scale analysis [11] the momentum Eq. (2) expresses the competition between three scales:

$$\rho\frac{u}{t},\ \rho u\frac{u}{r},\ \frac{P}{r}. \tag{2'}$$

In view of Eq. (3), the first two scales are both of order $\rho r/t^2$. In conclusion, the momentum Eq. (2) requires the following balance of two scales:

$$\rho\frac{r}{t^2} \sim \frac{P}{r} \tag{4}$$

Combining Eqs. (4) and (1), and neglecting (at this stage) factors of order 1, we conclude that the splat radius increases linearly in time,

$$r \sim Vt \tag{5}$$

This means that the splat radius moves outward with a speed of the same order as the speed of impact,

$$u \sim \frac{r}{t} \sim V \tag{6}$$

Let S be the cross-sectional area of the splat (in the plane of Fig. 2) at the time t, such that the conservation of droplet liquid volume requires

$$D^3 \sim rS \tag{7}$$

At this stage we do not know whether the splat is a flat disc or a ring: the shape of the splat will be determined next. The linear momentum of the droplet before impact is $(\rho D^3)V$. The linear momentum of the splat liquid is $(\rho Sr)U_a$ where U_a is the S-averaged radial velocity with which the splat liquid moves. The conservation of liquid linear momentum requires:

$$D^3 V \sim rSU_a. \tag{8}$$

Eqs. (7) and (8) require

$$U_a \sim V \tag{9}$$

According to Eq. (6), V is the velocity of the splat radius. Therefore, Eq. (9) states that *all* the splat liquid moves radially with the same speed as the splat radius, and from this follows the conclusion that the splat liquid must be located close to its rim. This is why in Fig. 2 the splat liquid is shown as a ring of radius r and cross-section S.

The length scale of the ring cross-section is $S^{1/2}$. This statement is equivalent to the assumption that the contact angle between the liquid–air surface and the solid surface is not infinitesimally small, i.e. that the shape of the ring cross-section S is not slender. This assumption covers most of the known liquid–air–solid contacts, which in the present scale analysis are represented by cross-sectional shapes (S) that have a single length scale ($S^{1/2}$), not two, a width

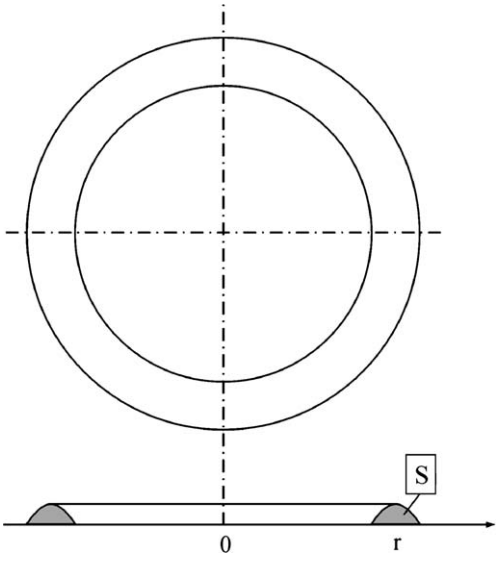

Fig. 2. Ring-shaped spreading of the liquid.

and a thickness. Next, by combining Eqs. (5) and (7) we find that the ring becomes thinner in time,

$$S \sim \frac{D^3}{tV} \tag{10}$$

Friction works toward slowing the spreading of the splat. The thickness of viscous penetration from the wall transversally through the splat is

$$\delta \sim (\nu t)^{1/2} \tag{11}$$

where ν is the liquid kinematic viscosity. The splat flow becomes viscid, and its spreading stops when viscous diffusion sweeps the entire splat cross-section. This happens when $\delta \sim S^{1/2}$, which in view of Eqs. (10) and (11) becomes the time scale

$$t_1 \sim \left(\frac{D^3}{\nu V}\right)^{1/2} \tag{12}$$

The splat radius at this time is

$$r_1 \sim \left(\frac{VD^3}{\nu}\right)^{1/2} \tag{13}$$

or

$$\frac{r_1}{D} \sim Re^{1/2} \tag{14}$$

where Re is the Reynolds number of the original droplet,

$$Re = \frac{VD}{\nu} \tag{15}$$

In conclusion, Eq. (14) shows that larger and faster droplets make relatively larger splats.

3. Splashing and needle-shaped flow

Next, we turn our attention to the effect of surface tension, and the stability of the circularly symmetric splat shape. According to Taylor's stability theory for a horizontal liquid layer of density ρ, with its free surface facing downward, and gravity acting downward, the wavelength λ that separates two adjacent droplets or jets is (Fig. 3)

$$\lambda \sim 10\left(\frac{\sigma}{\rho g}\right)^{1/2} \tag{16}$$

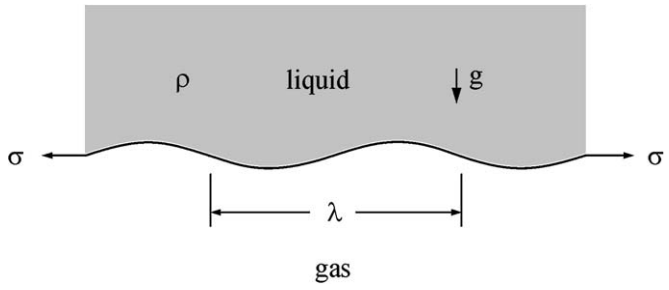

Fig. 3. The wavelength of Taylor instability.

Here 10 is the order of magnitude of the factor ($2\pi 3^{1/2}$ or $2\pi 6^{1/2}$) that appears in the exact solution to the stability problem [12]. In place of ρg, the force that pushes the splat liquid against the r-radius free surface is $P/r \sim \rho r/t^2 \sim \rho V/t$. Eq. (16) becomes

$$\lambda \sim 10\left(\frac{\sigma t}{\rho V}\right)^{1/2} \tag{17}$$

The wavelength of rim instability increases as $t^{1/2}$, whereas the rim radius increases as t, as shown in Fig. 4. At short times, r is smaller than λ, and the splat remains round. At sufficiently long times, the rim is long and flat enough to accommodate a ripple of several (n) wavelengths,

$$r \sim n\lambda \tag{18}$$

where n is a factor larger than 1, but not much larger, for example O(10). The time t_2 when Eq. (18) becomes true is estimated from Eqs. (17) and (18)

$$t_2 \sim (10n)^2 \frac{\sigma}{\rho V^3} \tag{19}$$

When $t_2 < t_1$, the splat develops a wavy rim before its motion is arrested by wall friction. This inequality is analogous to the comparison of two time scales that was used to predict flow morphology in Bénard convection, laminar-turbulent transition, and dendritic crystal growth [6,7]. By using Eqs. (12) and (19), we find that the splashing condition $t_2 < t_1$ can be written as

$$We^{1/2}Re^{1/4} > 10n = K \tag{20}$$

where We is the droplet Weber number,

$$We = \frac{\rho DV^2}{\sigma} \tag{21}$$

The splat ring radius at the time $t = t_2$ is

$$\frac{r_2}{D} \sim \frac{(10n)^2}{We} \tag{22}$$

If the inviscid splashing criterion (20) holds, then the liquid in the ring continues to flow radially outward in the form of n fingers. One such finger is sketched in

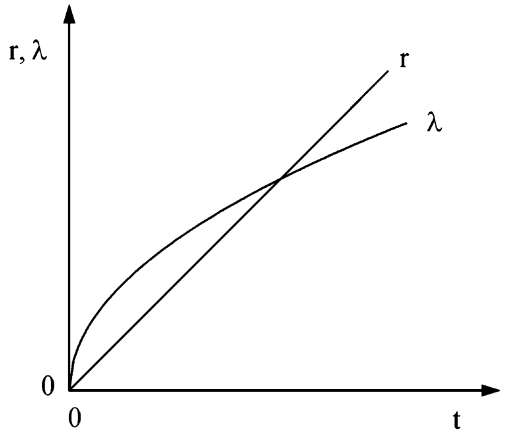

Fig. 4. The growth of the ring radius and the wavelength of Taylor instability.

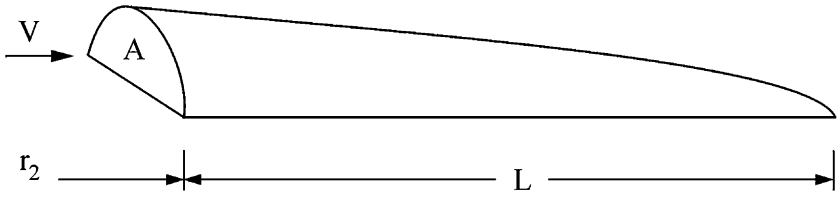

Fig. 5. Needle shape and parameters.

Fig. 5. The liquid enters with the velocity V through the $r = r_2$ end of the finger. Its bottom layers are slowed down viscously by the wall, while fresh liquid proceeds (over the top) to longer radial distances.

The farthest reach (L) can be estimated in two ways, as follows. Let A be the scale of the finger cross-sectional area, and $A^{1/2}$ the length scale of the finger cross-section. This is again the wettability assumption invoked above Eq. (10), according to which contact angles are not infinitesimally small, and the liquid cross-sectional shape has a single length scale ($A^{1/2}$), not two. The finger control volume is pushed from the left by the impulse $\rho V^2 A$, and from the right by the wall friction force,

$$\rho V^2 A \sim \tau L A^{1/2} \tag{23}$$

where $\tau \sim \mu V/AS^{1/2}$. In conclusion, the final length of the finger is

$$L \sim \frac{AV}{\nu} \tag{24}$$

Mass conservation requires $nSL \sim D^3$, and, after using Eq. (24), the dimensionless finger length becomes

$$\frac{L}{D} \sim \left(\frac{Re}{n}\right)^{1/2} \tag{25}$$

The time interval during which the finger grows is

$$t_3 \sim \frac{L}{V} \sim \frac{A}{\nu} \tag{26}$$

This t_3 expression suggests an alternative calculation of L: the finger length is the distance traveled by the V liquid during the time required by that liquid vein to be penetrated by viscous diffusion through its thickness $A^{1/2}$. That time is such that $A^{1/2} \sim (\nu t_3)^{1/2}$, which leads to Eq. (26) and, after invoking mass conservation, to Eq. (25).

To summarize, we determined the final length and time scales of a splat that remains ring shaped until its viscous death (r_1, t_1). We also determined the final length scale $(r_2 + L)$ and total time scale $(t_2 + t_3)$ of a round splat that splashes into n fingers. Taking the (r_1, t_1) scales as reference, we find that the ring and splash scales are of the same order of magnitude (see Eq. (20)):

$$\frac{r_2 + L}{r_1} \sim \frac{(10n)^2}{We\,Re^{1/2}} + \frac{1}{n^{1/2}} \sim 1 \tag{27}$$

$$\frac{t_2 + t_3}{t_1} \sim \frac{(10n)^2}{We\,Re^{1/2}} + \frac{1}{n^{1/2}} \sim 1 \tag{28}$$

Next, we make two additional observations in line with the constructal law of maximization of flow access, or acceleration of approach to equilibrium. First, the total splash time $(t_2 + t_3)$ can be minimized by selecting the number of fingers. The optimal number is

$$n_{\text{opt}} \sim \left(\frac{We\,Re^{1/2}}{4 \times 10^2}\right)^{2/5} \tag{29}$$

with the corresponding minimum splash time

$$\frac{(t_2 + t_3)_{\min}}{t_1} \sim \frac{5}{4^{4/5}} \left(\frac{10^2}{We\,Re^{1/2}}\right)^{1/5} \sim \frac{(r_2 + L)_{\min}}{r_1} \tag{30}$$

These results are order-of-magnitude accurate because they come from expressions (27), (28), which are based on scale analysis. Eqs. (29) and (30) can also be obtained in an order-of-magnitude sense by setting the two terms of Eq. (27) equal to each other. This alternate approach is the *intersection of asymptotes method*, which has been used several times in constructal theory to predict natural flow configurations, e.g., the first eddy of a turbulent flow, the onset of Bénard convection, the birth of needles in dendritic crystals and the characteristic length scale of cracks in volumetrically shrinking solids [6,7].

The second observation is that in view of the splash-formation criterion (20), the splash time is shorter than the ring time,

$$(t_2 + t_3)_{\min} < t_1 \tag{31}$$

If fingers can form, they *will* form, because fingers promise to bring the liquid to rest faster than the ring-shaped flow. This time minimization criterion is the same as the constructal law of maximization of flow access [6,7].

4. Dimensionless summary of ring and needle flows

One of the attributes of theory is that it organizes the presentation of the phenomenon in terms of the smallest and most relevant dimensionless groups. In this paper we have identified several length and time scales. If the post-impact flow of liquid is ring shaped (Fig. 2), then the time of the length and time scales when the growth of the ring is stopped by viscous diffusion are

$$\frac{r_1}{D} \sim Re^{1/2} \quad \frac{t_1 \nu}{D^2} \sim Re^{-1/2} \tag{32}$$

The time when the ring develops periodic deformations and fingers start to grow is characterized by the scales

$$\frac{r_2}{D} \sim \frac{(10n)^2}{We} \quad \frac{t_2 v}{D^2} \sim \frac{(10n)^2}{ReWe} \tag{33}$$

Dividing Eq. (33) by Eq. (32), we find how the scales of the beginning of splashing (r_2, t_2) are smaller than the scales of the ring-shaped droplet at the end of its symmetric growth (r_1, t_1):

$$\frac{r_2}{r_1} \sim \frac{t_2}{t_1} \sim \frac{(10n)^2}{WeRe^{1/2}} < 1 \tag{34}$$

These conclusions can be refined further by using the n_{opt} scale of Eq. (29) and introducing it in Eqs. (20) and (34). Accordingly, $K \sim 10n$ is

$$K \sim \frac{10}{400^{2/5}} We^{2/5} Re^{1/5} \tag{35}$$

Introducing this K estimate into the splashing criterion $t_2 < t_1$, or Eq. (20), we obtain

$$(We^{1/2}Re^{1/4})^{1/5} > \frac{10}{(400)^{2/5}} \sim 1 \tag{36}$$

We may compare this theoretical criterion with the experimental correlation [3]

$$(We^{1/2}Re^{0.25})^{1/5} > K^{1/5} \tag{37}$$

to see that $K = 57.7^{1/5} \sim 1$, which means that the theoretical criterion (36) agrees remarkably well with experimental data. To this comparison we will return in Table 2.

Another effect of the optimized number of needles becomes visible when we substitute Eq. (20) into Eq. (34):

$$\frac{r_2}{r_1} \sim \frac{t_2}{t_1} \sim \frac{100/(400)^{4/5}}{(WeRe^{1/2})^{1/5}} \sim \frac{1}{G} \tag{38}$$

where

$$G = (WeRe^{1/2})^{1/5} \tag{39}$$

Unlike $WeRe^{1/2}$, the new dimensionless group G has a *physical* meaning: G is the ratio of two lengths

$$G = \frac{\text{final radius of disc that dies viscously}}{\text{radius of still inviscid ring that just wrinkles}} \tag{40}$$

This is why $G \geqslant O(1)$ is the criterion for the occurrence of wrinkles on the rim at time t_2: the wrinkles grow as needles from t_2 to $t_2 + t_3$. On the other hand, when $G \leqslant O(1)$, the splat stops flowing when it is round, and consequently it has no future as a shape other than the round disc at rest.

Finally, to compare the scales of the splash 'just before' vs. 'end of splashing', we divide Eq. (30) by Eq. (38):

$$\frac{(r_2 + L)_{min}}{r_2} \sim \frac{(t_2 + t_3)_{min}}{t_2} \sim 5 \tag{41}$$

These ratios of length and time scales are the same constant which is on the order of 1. The size of the splashed droplet size is proportional to the size that the splat has at the start of asymmetric deformations. The fact that the ratios of length scales match the ratios of time scales, Eqs. (30) and (41), is a consequence of the constant velocity scale of the ring and finger fluid, V.

5. Experimental confirmation

The scaling laws uncovered in this paper are now compared with a set of experimental results published recently [5,13], where the experimental device was designed to record the shape evolution of droplets falling by gravity on solid substrates. Results are presented for millimetric droplets (1–3 mm in diameter) with relatively low velocities (1–4 m/s) and substrates of different roughness and wettability. The range of corresponding Reynolds numbers extends from 3500 to 12500, which corresponds to Weber numbers in the range 57–254.

The first theoretical result that we compare with experiments is the order of magnitude of the radial velocity U_a after impact. The analysis [Eq. (9)] shows that the initial radial velocity is on the order of the impact velocity. The experimental data available in Ref. [5] and displayed in Table 1 are for two impact velocities, $V = 1.2$ and 3.6 m/s. The tabulated data show that for both sets of experiments the ratio U_a/V is nearly constant. This means that Eq. (9) is verified, with a proportionality factor of 3.5 (with standard deviation of 10%), which is a factor on the order of 1.

Another important feature of the experimental data is that the ratio U_a/V is independent of the nature of the impact surface. This is in accord with the analysis that led to Eq. (9), which is based on the observation that the initial flow is inviscid, hence unrelated to the wall condition.

A systematic observation of the splat structure evolution was conducted in Ref. [5], by increasing step by step the impact velocity of droplets of the same diameter. The average value of the highest velocity for spreading and the lowest velocity for splashing yields a "transition" velocity, with a typical accuracy of 5%. Several substrates (glass, wax, PVC) and roughnesses ranging from 0.003 to 60 μm were used in the experiments, and this led to significant scatter in the results.

The values of the corresponding critical values for $We^{1/2}Re^{1/4}$ are shown in Table 2. Recall that We and Re are based on liquid properties and initial droplet diameter and velocity. In spite of the large scatter in the results, this table clearly shows the relevance of the group $We^{1/2}Re^{1/4}$ as

Table 1
Experimental measurements of the initial spreading velocity U_a: the tabulated values are for the ratio U_a/V (data from [5])

Substrate	$V = 1.2$ m/s	$V = 3.6$ m/s
Smooth wax	3.42	3.30
Smooth glass	3.45	3.21
Rough wax	3.98	3.49
Rough glass	3.84	3.21
PVC 300	3.41	3.69
PVC 100	3.38	3.63

Table 2
Experimental ranges of the transition between the spreading and the splashing regimes for several liquids and surface roughnesses (data from [5])

Liquid	D (mm)	V (m/s)	$We^{1/2}Re^{1/4}$	$G=(WeRe^{1/2})^{1/5}$
Water	3.44	1.55–3.15	90–220	6–8.7
Ethanol	2.80	1.26–1.85	90–146	6–7.3
Ethanol	1.34	1.58–2.67	69–133	5.4–7.1
Silicone oil	2.30	2.91	128	7

a transition parameter, because the order of magnitude of 10^2 is found for the transition in all the cases. As expected, the lower values (69–90) are found for the roughest surfaces. It is worth noting that the value given in Ref. [3] (namely $We^{1/2}Re^{0.25}=57.7$) is the lower bound of this range.

Table 2 also shows the corresponding values of G, which is the dimensionless transition criterion recommended by the arguments advanced in this paper, Eqs. (36) and (39). The experimental data collected in the table show that the transition is consistently associated with one G value, which is consistent with the transition criterion stated under Eq. (40).

Table 3 shows one more verification of the theory developed in this paper. The data are for a single droplet of initial velocity V and sphere diameter D, which impacts a surface perpendicularly and forms a splat that comes to rest as a disc. The observed final diameter of the disc is $D_{1,\mathrm{exp}}$. This dimension is compared with the theoretical scale r_1 shown in Eq. (13). Table 3 shows very good agreement between $D_{1,\mathrm{exp}}$ and r_1 for the first six cases tested: the ratio $r_1/D_{1,\mathrm{exp}}$ is on the order of one for each of the three liquids.

The seventh case (water) deviates somewhat from this pattern. The ratio $r_1/D_{1,\mathrm{exp}}$ is one order of magnitude greater than in the other three cases, meaning that the water splat comes to rest as a disc with a radius that is one tenth of the theoretical scale. This is a sign that the water splat departs from the model on which Eq. (13) is based. Because $D_{1,\mathrm{exp}}$ is smaller than r_1, it means that the water splat comes to rest under the action of a mechanism that is more effective as a transporter of momentum than the laminar shear flow of Eq. (13). The only more effective mechanism known is turbulent flow [7]. Indeed, the initial Reynolds number of the water droplet ($VD/\nu\sim 3000$) is the same as the Reynolds number of the initial radial flow of the deformed droplet. The value 3000 is two orders of magnitude greater than the Reynolds number for the onset of transversal waviness as in the fall of a film of condensate [11]. In the case of the splat, Fig. 1, the transversal waviness means concentric ripples, however, the value 3000 is high enough for the radial flow to be turbulent.

Table 3
Experimental measurements of the final diameter ($D_{1,\mathrm{exp}}$) of splats that come to rest shaped as a disc, and comparison with the theoretical scale of Eq. (13) (data from [5])

Liquid	ν (m^2/s)	σ (N/m)	V (m/s)	D (mm)	$D_{1,\mathrm{exp}}$ (mm)	$r_1/D_{1,\mathrm{exp}}$
Silicone oil	10^{-4}	21	0.89	2.84	4.5	1.6
Glycerin A	10^{-4}	63	0.97	2.08	2.7	1.72
Glycerin A	10^{-4}	63	0.96	2.64	3.9	1.70
Glycerin B	2×10^{-5}	64	1.05	1.95	3.4	2.9
Glycerin B	2×10^{-5}	64	1.98	1.92	4.2	3.14
Glycerin B	2×10^{-5}	64	2.75	1.84	5.3	3
Water	10^{-6}	73	0.90	2.71	6.4	10.5

A new theory defines the purpose of future experimental work. For example, it would be interesting to record in future experiments not only the final radius of the disc that dies viscously, but also the radius of the still inviscid ring at the time when it just begins to wrinkle. In this way the G ratio of Eq. (40) could be calculated, and the wrinkling criterion $G\geqslant \mathrm{O}(1)$ could be tested.

Another feature that deserves further study is the occurrence of turbulence in the flow of Fig. 1. This aspect illustrates another contribution of the theory: without theory, the seven cases shown in Table 3 recommend themselves as members of the same class. It is because of theory that we have the additional insight and incentive to search for turbulent flow features in disc-shaped splats before they die viscously.

6. Conclusion

In this paper we showed that the "sometimes round, sometimes crown" liquid droplets after impact can be reasoned as another manifestation of the constructal law. The flowing liquid chooses the configuration that maximizes its access, i.e. the architecture that allows it to flow the easiest and come to rest the fastest. The choice between round splats and splashing is dictated by the new dimensionless group G, which physically means a ratio of two length scales, cf. Eq. (40).

The most important message of this work is that, step by step, the constructal law brings under the tent of constructal theory a sequence of seemingly disconnected phenomena, which until now had only one feature in common: they had defied theory. Next to the examples with which constructal theory began (turbulence, mud cracks, coalescence of solid particles, round blood vessels, river cross-sections [6,7]), we now see the 23-level hierarchy of the human lung [8], the hydraulic jump [9], and 'evolutionary' dendritic flow patterns for heat and fluid flow [14,15]. These many examples illustrate the 'migration' that flow geometries exhibit in time, from nonequilibrium flow architectures to the equilibrium flow architectures that correspond to the existing global constraints [16].

The list of new applications of the constructal law is endless and deserves to be explored. Science itself is a *flow architecture*, which optimizes itself in time: the list of the unexplained becomes shorter thanks to the big tent offered by the new and successful theory. Only by getting better (compact, hierarchical, constructal) can observations keep on flowing into our finite-size brains. Only by getting better

(compact, hierarchical, constructal) can our brains maintain the outflow (science, knowledge), in spite of our finite-size anything (cranium, food, life time).

Acknowledgement

The authors wish to thank the Universities of Paris VI and Paris XI for inviting AB as a visiting professor at the FAST Laboratory.

References

[1] S. Haferl, D. Attinger, Z. Zhao, J. Giannakouros, D. Poulikakos, Transport phenomena in the impact of a molten droplet on a surface: macroscopic phenomenology and microscopic considerations. Part I: Fluid dynamics, Annu. Rev. Heat Transfer 11 (2000) 65–143.

[2] C.D. Stow, M.G. Hadfield, An experimental investigation of fluid flow resulting from the impact of a water drop with an unyielding dry surface, Proc. Roy. Soc. London A 373 (1981) 419–441.

[3] Chr. Mundo, M. Sommerfeld, C. Tropea, Droplet-wall collisions: experimental studies of the deformation and breakup process, Int. J. Multiphase Flow 21 (1995) 151–173.

[4] C. Escure, Etude de l'impact des gouttes d'alumine sur une cible chaude ou un film d'alumine liquide, Doctoral Thesis, University of Limoges, France, 2000.

[5] R. Rioboo, Impact de gouttelettes sur surfaces solides et séches, Doctoral Thesis, University Paris VI, 2001. Available from: <http://ftp.espci.fr/incoming/goutte/These_Rioboo.pdf>.

[6] A. Bejan, Advanced Engineering Thermodynamics, 2nd ed., Wiley, New York, 1997 (Chapter 13).

[7] A. Bejan, Shape and Structure, from Engineering to Nature, Cambridge University Press, Cambridge, UK, 2000.

[8] A.H. Reis, A.F. Miguel, M. Aydin, Constructal theory of flow architecture of the lungs, Med. Phys. 31 (5) (2004) 1135–1140.

[9] A. Pramanick, P.K. Das, Note on constructal theory of organization in nature, Int. J. Heat Mass Transfer 48 (2005) 1974–1981.

[10] A. Bejan, J.H. Marden, Unifying constructal theory for scale effects in running, swimming and flying animals, J. Exp. Biol. 209 (2006) 238–248.

[11] A. Bejan, Convection Heat Transfer, third ed., Wiley, New York, 2004, p. 454.

[12] J.H. Lienhard, A Heat Transfer Textbook, Prentice-Hall, Englewood Cliffs, NJ, 1981, pp. 399–400.

[13] R. Rioboo, C. Bauthier, J. Conti, M. Voué, J. De Coninck, Experimental investigation of splash and crown formation during single drop impact on wetted surfaces, Exp. Fluids 35 (6) (2003) 648–652.

[14] Z.-Z. Xia, Z.-X. Li, Z.-Y. Guo, Heat conduction optimization: high conductivity constructs based on the principle of biological evolution, in: 12th International Heat Transfer Conference, Grenoble, France, 18–23 August 2002, vol. 2, pp. 27–32.

[15] T. Borvall, A. Klarbring, J. Petersson, B. Tostenfelt, Topology optimization in fluid mechanics, in: H.A. Mang et al. (Eds.), Fifth World Congress on Computational Mechanics, Vienna, Austria, 7–12 July 2002.

[16] A. Bejan, S. Lorente, The constructal law and the thermodynamics of flow systems with configuration, Int. J. Heat Mass Transfer 47 (2004) 3203–3214.